THE JOURNAL OF CHEMICAL PHYSICS **138**, 12A524 (2013)

Single molecule probe reports of dynamic heterogeneity in supercooled *ortho*-terphenyl

Lindsay M. Leone and Laura J. Kaufman[a)]
Department of Chemistry, Columbia University, New York, New York 10027, USA

(Received 5 October 2012; accepted 17 December 2012; published online 11 January 2013)

The rotational dynamics of three perylene diimide dyes are studied on the single molecule (SM) level in *ortho*-terphenyl (OTP) near the glass transition temperature (T_g). At all temperatures probed, spanning 1.03–1.06 T_g, each of the three probes exhibits rotational correlation times, τ_c, that span more than a decade, consistent with the presence of spatially heterogeneous dynamics in OTP. No trend is found as a function of temperature, but a trend as a function of probe is observed: Average probe rotational correlation time scales inversely with breadth of SM τ_c distribution, with faster probes exhibiting broader τ_c distributions. This implies that dynamic exchange occurs on and below time scales associated with probe rotation. Extrapolating FWHM of rotational relaxation times to the structural relaxation time of the host shows that the τ_c distribution would span nearly two decades in the limit of no probe temporal averaging. Comparison with SM measurements in glycerol suggests that OTP demonstrates a greater degree of spatially heterogeneous dynamics in this temperature range than does glycerol. © *2013 American Institute of Physics*. [http://dx.doi.org/10.1063/1.4773889]

I. INTRODUCTION

Supercooled liquids are ergodic systems in the temperature range between the material's melting temperature and glass transition temperature (T_g), the point at which the system becomes non-ergodic. These materials lack long range order and exhibit high viscosity, often with that viscosity increasing in a non-Arrhenius manner with a decrease in temperature.[1–3] Fundamental aspects of these systems have been a topic of interest for decades, but the nature of molecular motions within supercooled liquids remains poorly understood. In recent years, it has been demonstrated that supercooled liquids display spatially heterogeneous dynamics, in which molecules exhibit different dynamical behavior as a position of space (spatial heterogeneity) and/or time (temporal heterogeneity) in the system.[4,5] These spatially heterogeneous dynamics exist even though supercooled liquids appear to lack static, structural heterogeneity. The length and time scales that characterize spatially heterogeneous dynamics in supercooled liquids remain an area of debate, as does the related question of whether a growing length scale associated with cooperatively rearranging regions governs dynamics in these systems as the temperature is lowered towards T_g.[6,7] Elucidating the particular time and length scales of such heterogeneous behavior and addressing the related question about a potentially temperature dependent length scale of cooperative dynamics may help distinguish between the various theories that have been proposed to explain the glass transition.[8]

Given the presumed spatially heterogeneous nature of supercooled liquids, traditional techniques that interrogate a large ensemble of molecules necessarily average over spatial, and potentially temporal, heterogeneities in such systems. Novel methods to avoid full ensemble averaging and interrogate sub-ensembles of molecules have been developed and employed to provide insight into the degree of heterogeneity in small molecule supercooled liquids.[4,5,9,10] To limit spatial averaging as much as possible and interrogate molecular length scales in these systems, single molecule (SM) approaches have been employed.[11–14] The SM technique that has been most commonly applied to the study of supercooled liquids involves embedding fluorescent probes very dilutely into the host under study and monitoring SM probe rotations over time through measurement of probe linear dichroism (LD). In theory, these experiments can identify both spatial and temporal heterogeneity in supercooled liquids through analysis of differences between individual SM probe behavior (spatial heterogeneity) and differences in behavior that occur for a given SM over time (temporal heterogeneity). Identifying temporal heterogeneity and distinguishing spatial and temporal heterogeneity have proven more difficult in practice, due in large measure to typical SM probe characteristics.[15] First, SM probes are usually large, and their rotations are slow compared to molecular motion of the host molecules. It is likely that dynamic exchange—the changes in dynamics of particular regions of the supercooled liquid over time—occurs on time scales that are faster than and/or not well separated from probe rotational time scales, thus limiting probe ability to report these dynamics. Moreover, typical SM probes photobleach on time scales that limit trajectory length, which affects the accuracy of variables obtained from fitting correlation functions derived from these trajectories. It may be expected that a SM LD trace analyzed via an autocorrelation function (ACF) would yield a single exponential decay if the probe were experiencing an environment of given dynamics but would yield a stretched exponential decay for

a)Author to whom correspondence should be addressed. Electronic mail: kaufman@chem.columbia.edu.

a SM that explored multiple such environments. Unfortunately, typical SM LD trajectories are short enough such that they may be best fit by stretched exponential decays even in the presence of homogeneous dynamics.[16,17] This complication requires that temporal heterogeneity be identified with other approaches, and several such approaches have been developed.[12,13,18–20] However, these approaches typically yield information on time scales much longer than the structural, or α-, relaxation time, τ_α, of the host, a time scale that has been has been suggested to be similar to that of dynamic exchange at temperatures near T_g.[21–23]

To potentially identify temporal heterogeneity and quantify dynamic exchange on shorter time scales, a recent study monitored the rotational dynamics of a set of three SM probes.[14] In this study, performed in supercooled glycerol, the largest probe employed unexpectedly displayed the shortest rotational correlation time, likely because steric hindrance prevented it from participating in glycerol's hydrogen-bonding network. A key observation of this study was the faster the probe's average rotational correlation time, regardless of probe size, the broader the distribution of individual SM probe rotational correlation times. We hypothesized that the most quickly rotating probe reported the greatest breadth of heterogeneity in the host because it did less averaging over dynamic exchange in the system, allowing it to more faithfully report the spatially heterogeneous dynamics of the surrounding supercooled glycerol than could the slower probes.

The results of this study of SM probes in supercooled glycerol lead to predictions for how these probes will behave in other supercooled liquids. In this paper, we test those predictions and use probe-dependent SM studies to detail aspects of the spatially heterogeneous dynamics of *ortho*-terphenyl (OTP). Unlike glycerol, OTP is non-polar and is expected to have very similar molecular interactions with all employed probes. As such, we propose that in OTP, unlike in glycerol, the probes will have rotational relaxation times governed by probe size, and the largest probe will be the slowest. As in glycerol, we expect the probes in OTP will show increase in breadth of rotational relaxation time distribution with decreasing average probe rotational correlation time, consistent with fast probes doing less averaging over and better reporting of dynamic exchange occurring in the host. Because OTP is a more fragile glass former than glycerol, and fragility may be correlated with the degree of heterogeneous dynamics in a glass former,[4,24] we will examine whether results from these studies suggest differences in the relative heterogeneity of glycerol and OTP.

In particular, in this study OTP is doped with 3 perylene diimide (PDI) probes, 2 of which were used in the previously mentioned glycerol study.[14] Individual probes' rotational correlation times are measured at temperatures in the range of 1.03–1.06 T_g. The distributions of rotational correlation times as a function of temperature and probe are reported. Individual correlation functions are also combined into a quasi-ensemble for comparison to results of ensemble measurements of supercooled OTP. Results in OTP are compared to previously collected data in glycerol to assess relative heterogeneity of these two glass formers.

II. EXPERIMENTAL

A. Sample preparation

Ortho-terphenyl (Fluka, spectrophotometric grade) is vacuum-distilled three times and then dissolved in toluene (Sigma Aldrich, spectrophotometric grade) to obtain a 5.0 mg/ml solution. This solution is photobleached in a home-built bleaching apparatus for 48 h.[25] Solid *N,N′*-bis(2,6-dimethylphenyl)-3, 4, 9, 10-perylenedicarboximide (dpPDI) and *N,N′*-bis(2,5-tert-butylphenyl)-3, 4, 9, 10-perylenedicarboximide (tbPDI) are obtained from Sigma Aldrich. Solid *N,N′*-bis(triethylglycol)-3, 4, 9, 10-perylenedicarboximide (egPDI) is synthesized and generously provided by L. Campos and co-workers in the Department of Chemistry at Columbia University. dpPDI, tbPDI, and egPDI are provided as solids and are dissolved in toluene to form stock solutions that are ultimately diluted to $1.0–5.0 \times 10^{-8}$ M for use in SM imaging. At these concentrations, fluorophores are dilute enough to avoid multiple SMs within a diffraction limited spot but concentrated enough to yield 50–200 analyzable SMs per movie.

Phenylsilane treated silicon wafers are sonicated in acetone for 10 min at least twice, rinsed in toluene, and briefly dried on a hot plate at 100 °C. This process enhances wetting and film stability of OTP on the wafer. The PDI/OTP solutions are spin coated onto these silicon wafers at 200 rpm, until the toluene has evaporated and a lustrous film forms. After the film has formed, spinning continues for ∼10 additional seconds. The spin-coating is performed at room temperature, ∼50 K above OTP's glass transition temperature (T_g = 243 K). The OTP films produced are ∼500 nm and rather flat across the sample as judged by interference fringes.

The sample is placed into a liquid nitrogen cooled microscopy cryostat, and vacuum grease is applied to the sample stage to optimize thermal contact between the sample wafer and cryostat stage. The cryostat stage temperature is initially set to 285 K to facilitate rapid cooling of the sample upon contact. Once the sample is placed into the cryostat, the stage temperature is lowered to the desired temperature (250–258 K, 1.03–1.06 T_g) at a rate of ∼5 K min^{-1}. Upon beginning sample cooling, the cryostat is evacuated to ∼30 mTorr and flushed with dry nitrogen 5 times. The cryostat is then evacuated to 0.4 mTorr for at least 1 h to ensure all toluene has been removed from the sample. The temperature control system is outlined in detail in Ref. 13.

B. Optical setup

Data are acquired using a home built microscope in an epi-fluorescence configuration (Fig. 1). This configuration is similar to the one described previously.[13] One change has been made to the previously described experimental setup to allow for a more homogeneously illuminated field of view: approximately 150 mW of excitation light (from an Nd:Vanadate 532 nm diode laser) is directed into an objective lens and coupled into a multimode fiber (Newport, F-MCB-T-3FC) that is shaken by a piezoelectric buzzer at 500-4700 Hz (MCM Electronics; PEB in Fig. 1) to eliminate

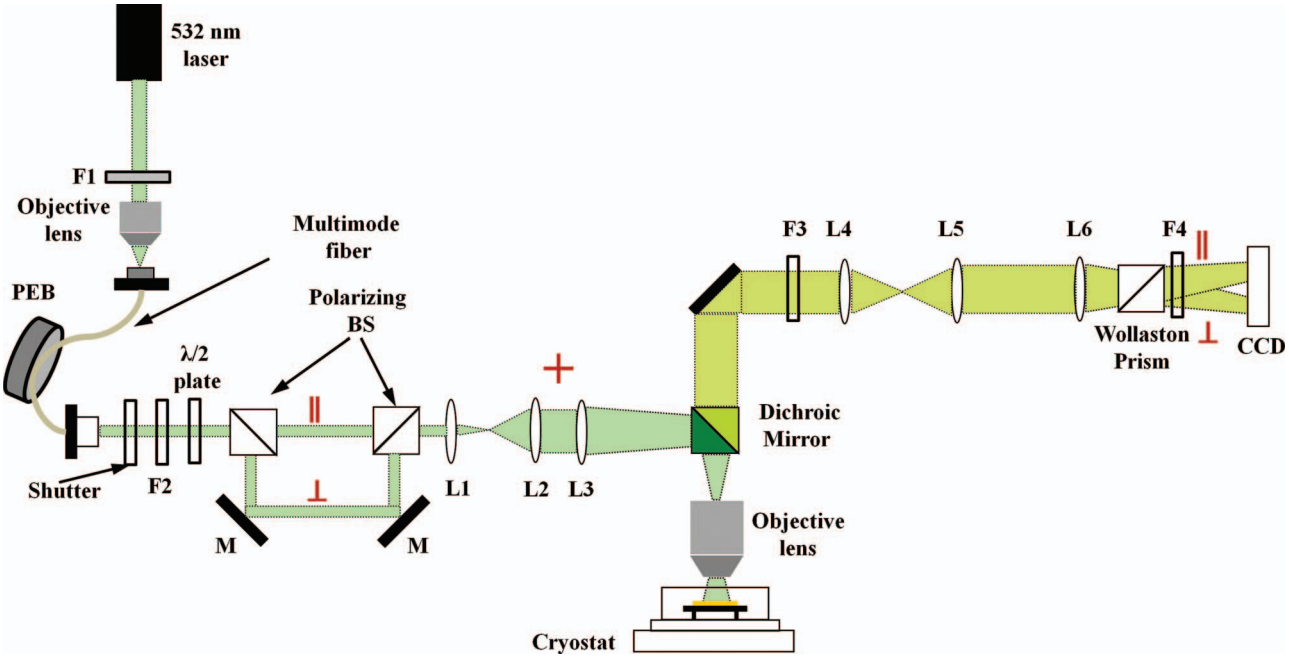

FIG. 1. Schematic diagram (not to scale) of the epi-fluorescence microscope. BS = beam splitter, F = filter, M = mirror, PEB = piezoelectric buzzer, L = lens.

the speckle pattern produced by multimode fibers. The unpolarized light is directed out of the fiber via a collimator and is passed through polarization optics and a telescope before being reflected towards the objective lens.

The fluorescence from SMs in the illuminated area is collected by a long working-distance, high numerical aperture objective (Zeiss, LD Plan-Neofluar, air 63x, NA = 0.75, WD = 1.5 mm), passed through detection optics including a Wollaston prism that splits the signal into two orthogonal polarizations and onto an electron multiplying charge-coupled device camera (Andor iXon DV887; EMCCD in Fig. 1). Data are collected at temperatures from 250 to 258 K. The optimal frame rate of each movie is determined based on preliminary experiments, and ≈20 frames per median rotational relaxation time, $\tau_{c,med}$, are collected at each temperature for each probe. Trial movies are also collected at both faster and slower frame rates to search for molecules whose rotations cannot be quantified with the chosen frame rate—in this paper movies collected at additional frame rates are not found necessary, and all molecules described are from movies collected at the typical frame rate. Measurements are taken for several thousand frames, until >95% of the SMs have photobleached. For measurements taken at 20 Hz, 10 Hz, and 5 Hz, the sample is continuously illuminated, and the exposure time is the inverse of the frame rate. At lower temperatures, measurements are taken at 2 Hz, 1 Hz, 0.5 Hz, and 0.25 Hz with a fixed exposure time of 0.2 s. The laser is shuttered with a mechanical shutter for the remainder of the frame time to limit photobleaching. The laser power used to collect data ranges from 0.75 to 30 mW, as measured before the objective lens. The highest powers are required at the highest frame rates. Signal-to-noise ratio (SNR) for all movies is at least 2. To allow for correction of heating due to absorption of laser light, movies are collected at several powers at a given temperature for a given sample. Median probe rotational correlation time as a function of set temperature and laser power is used to extrapolate an actual temperature for each sample, as described in Ref. 14.

In all, 156 movies were collected and analyzed, 53 for dpPDI, 36 for egPDI, and 60 for tbPDI. The number of data sets collected at each temperature for each dye can be ascertained from Fig. 2 where each data point represents the median rotational relaxation of probe molecules in a single movie. The number of molecules analyzed for each PDI dye at each temperature is given in Table I. Data was collected over a 4 day period on two different samples for each PDI dye in OTP. During data collection, temperature was varied at random over the full range of measured temperatures.

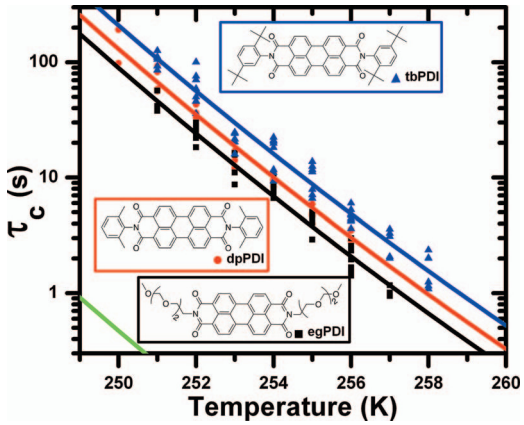

FIG. 2. Rotational relaxation times vs. temperature for tbPDI (blue triangles), dpPDI (red circles), and egPDI (black squares) together with each dye's molecular structure outlined in the same color. Each point represents the heat corrected $\tau_{c,med}$ value for a single movie. Lines represent the best-fit DSE fit for each PDI dye. Extracted hydrodynamic radii are $V_h = 1.87$ nm^3 (tbPDI), $V_h = 1.17$ nm^3 (dpPDI), and $V_h = 0.80$ nm^3 (egPDI). The structural relaxation of OTP as measured by dielectric spectroscopy[30] is plot as a function of temperature (green line).

TABLE I. Number of molecules and FWHM values of best-fit Gaussian distributions of $\log(\tau_c)$ values for all SM data shown in Fig. 3, left panel. Average FWHM over all temperatures as a function of probe as well as the FWHM values for the combined histograms shown in the right panel of Fig. 3 are also given.

	tbPDI		dpPDI		egPDI	
T/K	Molecules	FWHM	Molecules	FWHM	Molecules	FWHM
250	...	...	444	0.71	...	...
251	402	0.60	524	0.66	327	0.65
252	582	0.61	534	0.57	458	0.70
253	655	0.48	567	0.63	316	0.62
254	613	0.64	1117	0.61	462	0.73
255	509	0.61	619	0.62	468	0.71
256	969	0.51	822	0.59	477	0.70
257	599	0.35	...	...	493	0.73
258	513	0.60	...	...	...	...
Average		0.55		0.63		0.69
Combined	4842	0.54	4627	0.61	3001	0.69

In the Discussion, SM data collected in OTP is compared to data collected in glycerol that was reported and described in Ref. 14. Sample preparation and data analysis is described in that publication and is very similar to that outlined here. In that study, tbPDI and dpPDI were employed. The third probe used in that study was *N,N′*-bis[3-dimethylamino)propyl]-3, 4, 9, 10-perylenedicarboximide (dapPDI).

C. Data analysis

Data analysis is performed using IDL software (ITT Visual Information Solutions), as described in detail in Ref. 13. Features are identified and the intensity of each SM is extracted as described in that publication. The linear dichroism $LD = \frac{I_\parallel - I_\perp}{I_\parallel + I_\perp}$ is calculated, and an autocorrelation function $ACF = C(t) = \frac{\sum_{t'} a(t')a(t'+t)}{\sum_{t'} a(t')a(t')}$ with $a(t) = LD(t) - \langle LD(t)\rangle$ is constructed from the LD. Each ACF is fit with least squares fitting until the correlation function decays to 0.1 with a stretched exponential decay $C(t) = Ae^{-(t/\tau_{fit})^\beta}$, where β is the stretching exponent. For these fits, β values are constrained to $0.3 \leq \beta \leq 2.0$. The extracted relaxation time is given by $\tau_{\text{str exp}} = \frac{\tau_{fit}}{\beta}\Gamma(\frac{1}{\beta})$, where $\tau_{\text{str exp}}$ represents the mean relaxation time extracted from that ACF.

Because it has been shown that trajectory length affects accuracy of extracted relaxation time (as well as β value), although all ACFs are initially fit with a stretched exponential, $\tau_{\text{str exp}}$ is not necessarily considered to be τ_c.[13,26] For trajectories with >20 points per $\tau_{\text{str exp}}$ and trajectory length <50 $\tau_{\text{str exp}}$, a linear fit is found to be more accurate. Here, the early portion of the ACF is fit with $mt + b$, and b/m is considered to be τ_c. For all other trajectories, $\tau_{\text{str exp}}$ is considered to be τ_c. This treatment is performed for all molecules in a given movie, and a τ_c value is extracted for each SM. A median τ_c, $\tau_{c,\text{med}}$, is also found for each movie. Due to potential heating from laser absorption, an iterative heating correction outlined in Ref. 14 is applied to determine a true temperature and potentially adjust all τ_c values to the set temperature. For evaluation of SM stretching exponents, all SMs (regardless of whether τ_c is determined from a stretched exponential or a linear fit) are fit to a stretched exponential function, and β is recorded.

D. Heating correction

In the supplementary information of Ref. 14, the heating correction applied to SM data collected in glycerol was described in detail. That same procedure is used here to find both true temperature of the sample for each movie or, alternately, heat corrected τ_c values for each data point. Unless otherwise stated, all τ_c values presented and described are heat-corrected. The temperature dependent viscosity data for OTP used to perform the heat correction is given in Ref. 27. In this paper a second, nearly identical heating correction is performed to obtain relative time scales of probe and host relaxation dynamics as characterized by probe rotational correlation time and host structural relaxation time, τ_c/τ_α. This procedure is described in the supplementary material.[28]

E. Simulations

For comparison to experimental results, simulations of 3D rotational diffusion of a unit vector representing the transition dipole of a fluorophore are performed as described previously.[13,17] The rotational diffusion constant, D_r, and rotational correlation time, $\tau_c = 1/6D_r$, are set by choosing the average angle by which the unit vector rotates per step. The dipole orientation is used to calculate the parallel and perpendicular fluorescence intensities assuming wide-field excitation and detection with a NA = 0.75 objective, in analogy with the experimental configuration. LD is calculated from the two orthogonal intensities and 30% Gaussian noise relative to the mean signal is added for consistency with experimental data. Simulations are constructed with median τ_c of 20 steps and are varied in length to match the average length for a given probe molecule in OTP (Table II). For all simulations, as for experiments, LD ACFs are constructed from the LD and are fit as outlined in Sec. II C to yield a τ_c value. Trajectories treated with linear fits are also fit with stretched exponentials to yield a β value, as is also done with experimental trajectories.

TABLE II. Various quantities for experiments and simulations for the three employed probes in OTP. Lifetime/τ_c is determined for each movie as the average time each SM is "on" (typically the time until photobleaching) divided by the average τ_c value for that movie. These quantities are then averaged. FWHM, β_{med}, and β_{QE} are experimental quantities as described in the text and shown in Figs. 3 and 4. FWHM_{sim}, $\beta_{\text{med,sim}}$, and $\beta_{\text{QE,sim}}$ are quantities obtained from simulation as described in the text and shown in Figs. 3 and 4.

Dye	Lifetime/τ_c	FWHM	FWHM_{sim}	β_{med}	$\beta_{\text{med,sim}}$	β_{QE}	$\beta_{\text{QE,sim}}$
tbPDI	46	0.55	0.35	1.08	1.08	1.01	1.03
dpPDI	38	0.63	0.39	1.04	1.11	0.96	1.02
egPDI	96	0.69	0.34	0.94	1.03	0.78	1.04

III. RESULTS

A. Median rotational relaxation times

We first investigate the temperature dependence of measured SM probe dynamics, on average, in OTP. In particular, we investigate whether median rotational correlation times of the probe molecules track the temperature dependence of the host viscosity as described via the Debye–Stokes–Einstein (DSE) equation,

$$\tau_c = \frac{V_h \eta(T)}{k_B T}, \quad (1)$$

where τ_c is the rotational relaxation time of the probe, V_h is the hydrodynamic volume of the probe, η(T) is the temperature dependent viscosity of the host, k_b is the Boltzmann constant, and T is temperature of the host. Previous SM measurements have found that the DSE equation does describe probe rotational dynamics in small molecule supercooled liquids.[11,12,14] We use the DSE equation not only to help establish that probe dynamics reflect host dynamics but also to extract an effective hydrodynamic volume, V_h, for each probe.

Using the heating correction algorithm based on the measurements taken at different powers, a single median τ_c, $\tau_{c,med}$, is obtained from each movie for a given probe. These $\tau_{c,med}$ values are fit to the DSE equation using the known temperature dependence of OTP viscosity[27] (Fig. 2). In Figure 2, each point represents the $\tau_{c,med}$ value for a single movie containing 50-150 molecules. Each line corresponds to the DSE line of best fit for each probe's $\tau_{c,med}$ values with respect to temperature. The extracted hydrodynamic volumes for tbPDI, dpPDI, and egPDI in OTP are $V_h = 1.87\ nm^3$, $V_h = 1.17\ nm^3$, $V_h = 0.80\ nm^3$, respectively. This reflects the fact that of the three probes at a given temperature in OTP, tbPDI rotates the slowest and egPDI rotates the fastest.

B. Degree of spatially heterogeneous dynamics

1. Breadth of relaxation times

After evaluating the average dynamics of the three PDI dyes in OTP, we assess information attained from individual SM linear dichroism auto-correlation functions for all PDI dyes at each temperature probed. First, heat corrected τ_c values obtained from every individual SM are plot in histograms at each temperature ranging from 250 to 258 K for each PDI dye (Fig. 3, left panel). There is a substantial spread in relaxation times for all probes at all temperatures investigated, with each histogram spanning over a decade.

Each distribution of rotational correlation times is plot on a log scale and fit with a Gaussian function given by

$$y = Ae^{-\frac{(x-x_c)^2}{2\sigma^2}} + y_0; \quad \text{FWHM} = (2\sqrt{2\ln 2}\sigma). \quad (2)$$

The distributions are also fit to a Lorentzian curve given by

$$y = \frac{A\gamma}{(x-x_c)^2 + \gamma^2} + y_0; \quad \text{FWHM} = 2\gamma. \quad (3)$$

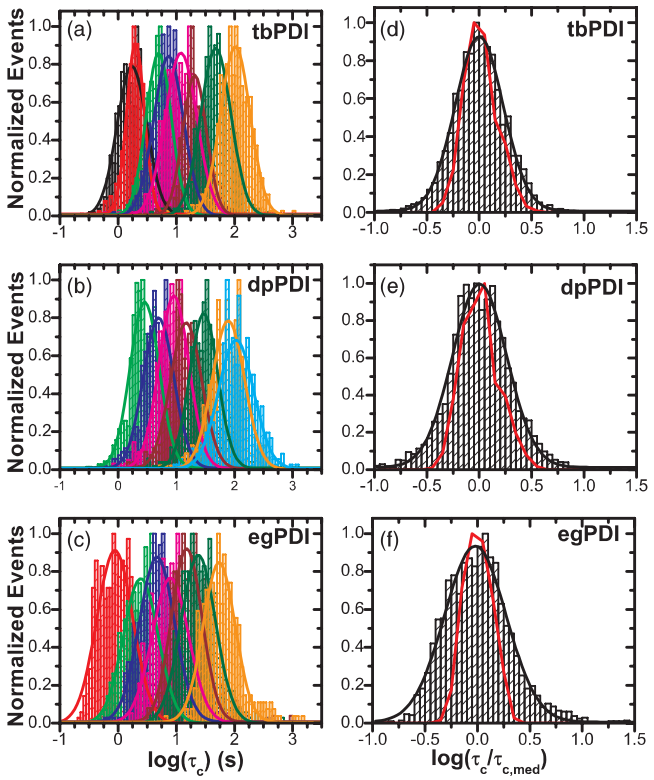

FIG. 3. (Left) Distribution of SM τ_c values for (a) tbPDI, (b) dpPDI, and (c) egPDI in OTP at 258 K (black), 257 K (red), 256 K (green), 255 K (blue), 254 K (magenta), 253 K (wine), 252 K (olive), 251 K (orange), and 250 K (cyan). All histograms are normalized to the maximum number of occurrences. Each histogram is taken from two data sets for each dye, with the histograms across data sets normalized to the median τ_c value of one of the data sets for that particular PDI dye. This alleviates any potential widening of the distribution arising from differing thermal contact of the sample and stage between data sets. (Right) SM data from all temperatures normalized by $\tau_{c,med}$ and combined to form a single histogram for (d) tbPDI, (e) dpPDI, and (f) egPDI. Each histogram is fit with a Gaussian function (black line). Histogram of τ_c distribution of simulations of homogeneous rotational diffusion with trajectory length for each simulation tuned to match average experimental trajectory length as described in the text is shown by the red lines.

In both cases, fits allowing all variables to float and fits fixing the height to 1 and offset to 0 are performed. As judged by R^2 values, Gaussian fits with floating variables provide the best fits and these are shown in Fig. 3. FWHM values are reported in Table I. For all four types of fits, the FWHM values extracted show the same trend, with the egPDI τ_c distribution having the largest FWHM and tbPDI the smallest.

Regardless of particular fitting procedure, no obvious trend is found for width of the distribution as a function of temperature for any of the probes. As such, in addition to plotting τ_c distributions for each probe at each temperature (Fig. 3, left panel), a normalized τ_c distribution for all temperatures is constructed (Fig. 3, right panel). These histograms are also fit to Gaussians and Lorentzians with and without constraints as described above. Again, Gaussian fits provide better fits than Lorentzians (for variable amplitude fits, $R^2 \geq 0.98$ for Gaussians vs. $R^2 \geq 0.95$ for Lorentzians). The FWHM values extracted from the combined-temperature distributions are very similar to the average FWHM values for a particular probe's distribution across temperatures (Table I).

Moreover, the trend showing $FWHM_{egPDI} > FWHM_{dpPDI} > FWHM_{tbPDI}$ for τ_c distributions at individual temperatures also holds for this combined data.

For all probes, at all temperatures, the observed τ_c distributions are broader than would be expected for a normal liquid, even given the experimental constraint of short trajectories. Simulations of 1000 trajectories of homogeneous rotational diffusion, all with the same τ_c, were performed with trajectory length set to average trajectory length for each of the probe molecules in OTP: $46\tau_c$, $38\tau_c$, and $98\tau_c$ for tbPDI, dpPDI, and egPDI, respectively (Table II). In all cases, the simulations yield distributions (red lines, Fig. 3, right panel and Table II) narrower than those measured experimentally, though broadened relative to the delta functions that would be expected for infinitely long trajectories. Performing simulations such that the trajectory length distribution (rather than simply the average trajectory length) matches that of experimental results yields very similar distributions, with a FWHM a maximum of 3% larger than that obtained using average trajectory length. We note that egPDI is the broadest of the three experimental distributions but would be expected to have the narrowest distribution in the absence of spatially heterogeneous dynamics since it has the longest trajectories. The experimentally recorded spread of τ_c values confirms that spatially heterogeneous dynamics exists in supercooled OTP and that all probes used in this study report on these heterogeneous dynamics.

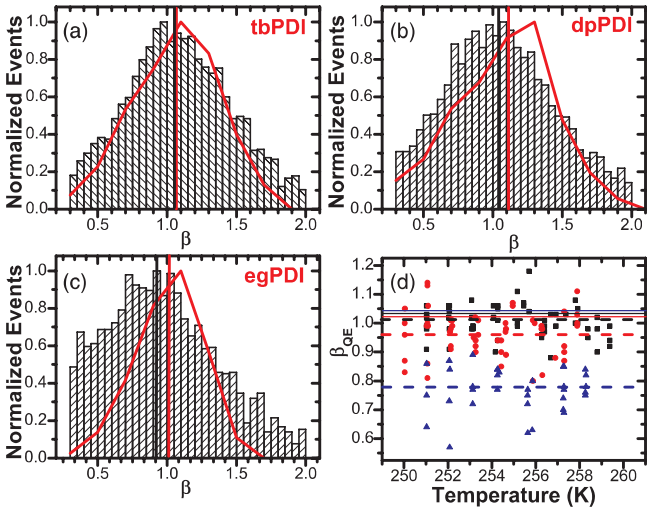

FIG. 4. Distributions of β values from individual SM ACF fits for (a) tbPDI, (b) dpPDI, and (c) egPDI. The solid black lines indicate the median value, β_{med}, of these distributions. The red curve represents distributions from simulations of homogeneous rotational diffusion with trajectory length set to match average experimental trajectory length. For all experimental and simulated data, β is allowed to float from 0.3 to 2.0 when each ACF is fit with a stretched exponential as described in the text. (d) β_{QE} values for each probe for each movie collected as a function of true temperature for tbPDI (black squares), dpPDI (red circles), and egPDI (blue triangles). The dashed lines of corresponding color represent the mean β_{QE} value for each probe for all temperatures studied. The solid lines of corresponding color represent the β_{QE} values from the corresponding simulations.

2. Evaluation of stretching exponent

In bulk experiments, which cannot access distributions of individual relaxation times as described above for SM probes, exponents derived from stretched exponential fits of ensemble ACFs of a variety of observables have been used to assess degree of spatially heterogeneous dynamics in supercooled liquids. In SM experiments, stretching exponents can also be assessed, both from individual SM ACFs as well from quasi-ensemble ACFs constructed from SM ACFs.

As described in the Introduction, time-limited trajectories may display ACFs with best-fit stretching exponents differing from 1.0 even for systems displaying homogeneous rotational dynamics, with strong effects still seen for trajectories 100 times longer than the characteristic rotational correlation time,[16,17] longer than the typical trajectories recorded here. For this reason, attributing the small stretching exponent of a given SM ACF to that SM probe experiencing different dynamic environments over the course of the experiment is not advisable.[15] Distributions of β values across SM ACFs are also affected by short trajectories but may yield some information about degree of heterogeneity in a supercooled liquid. Figure 4 shows the distributions of β values for all individual SM traces, each of which was fit to a stretched exponential decay, for each of the three probes. β is allowed to float from 0.3 to 2.0 when each ACF is fit with a stretched exponential. Tails at 0.3 and 2.0 are removed from the figures and not included in the calculation of β_{med}. The difference in β_{med} with and without tails included is less than 1%. Fits were also performed allowing β to float from 0 to 2.0 when fitting ACFs of egPDI in OTP, and this results in $<2\%$ difference in the β_{med} value. As with the τ_c value distributions, the distributions of and median β values do not show any clear trend with temperature (data not shown); therefore, these distributions are constructed using data for all temperatures. A median stretching exponent, β_{med}, is determined from these distributions: the β_{med} values are 1.08, 1.04, and 0.94 for tbPDI, dpPDI, and egPDI, respectively. We estimate the error on these values as $<\pm 0.01$ as follows: least squares fitting of individual LD ACFs yields scaled uncertainties for β of approximately ± 0.2; propagating error through calculation of the average for a given movie yields β_{med} error of ± 0.02–0.04 and then is reduced further by averaging over all movies. The β_{med} values are shown as solid black lines in Fig. 4 and are reported in Table II.

Figures 4(a)–4(c) also show distributions of β values for the simulations of homogeneous rotational diffusion described above, with trajectory length set to average trajectory length for each of the probes. In all cases, the simulation data are treated as the experimental data and yield distributions that are somewhat different than the experimental distributions, with the simulated distributions somewhat narrower than the experimental ones. Unlike for the τ_c distributions, where the experimental FWHM values are distinct from those yielded by simulation, the overall experimental and simulated distributions of β values and the β_{med} values are quite similar, particularly for tbPDI and dpPDI. These results suggest that the time-limited nature of typical trajectories affects individual SM ACF β values such that neither a particular β value nor the full distribution of an ensemble of SM β values

TABLE III. Molecular weight (MW), extracted hydrodynamic volumes (V_h), van der Waals volume (V_v), V_h/V_v ratios, and τ_c/τ_α values as described in the text for the three probes investigated in OTP and in glycerol.[14]

Probe	MW (g/mol)	V_V (nm^3)	$V_{h\,(OTP)}$ (nm^3)	$V_{h\,(OTP)}/V_V$	$V_{h\,(glycerol)}$ (nm^3)	$V_{h\,(glycerol)}/V_V$	$\tau_c/\tau_{\alpha,OTP}$	$\tau_c/\tau_{\alpha,glycerol}$
tbPDI	766.38	0.67	1.87	2.77	0.36	0.53	297	14
dpPDI	598.65	0.46	1.17	2.54	2.02	4.39	193	66
egPDI	684.73	0.54	0.80	1.48	...	...	168	...
dapPDI	560.64	0.45	...	...	1.27	2.82	...	42

can necessarily discriminate between a homogeneous and heterogeneous population.

Another method that allows evaluation of SM data for indications of host temporal heterogeneity as well as comparison to bulk experiments requires construction of a quasi-ensemble ACF (ACF_{QE}). As described in Ref. 17, for each movie all individual SM ACFs are summed to produce a single ACF_{QE}, which is fit with a stretched exponential function. Each ACF_{QE} yields a τ_{QE} and a β_{QE} value. The τ_{QE} values can be used in much the same way the $\tau_{c,med}$ values are used to extract a V_h for each probe. Doing so leads to the following V_h values: 1.82, 1.15, and 0.87 nm^3 for tbPDI, dpPDI, and egPDI, respectively—a maximum of 11% difference from the results obtained with the approach represented by Fig. 2. This similarity validates the use of the ACF_{QE}s for data analysis. The quasi-ensemble stretching exponents, β_{QE}, are shown for each probe as a function of true temperature in Fig. 4(d). While τ_c values can be heat-corrected using the DSE curve as a guide, ACFs cannot be straightforwardly heat-corrected. Because multiple movies collected at the same set temperature may have different degrees of heating, data across movies cannot be combined in constructing ACF_{QE}s, and therefore these ACF_{QE}s are constructed from SMs in a single movie. The obtained β_{QE} values, again, show no clear trend with temperature, while a trend as a function of probe is apparent. The mean β_{QE} values obtained for tbPDI, dpPDI, and egPDI are 1.01, 0.96, and 0.78 respectively (Table II). The scaled uncertainly for the β_{QE} value for each movie is ±0.02–0.04; thus, the error bars are around the size of the data points in Fig. 4(d). The average β_{QE} error is lower by approximately an order of magnitude; however, as discussed below, scatter between points representing different movies exists in part due to differences in average trajectory length of the movies. Average β_{QE} values for each probe are lower than the β_{med} values in all cases. This result stands in contrast to results for simulations, where β_{QE} values obtained from the same simulations used to construct the distributions of τ_c and β values shown in Figs. 3 and 4 are very similar to the β_{med} values and very close to 1.0 (Figure 4(d) and Table II).

IV. DISCUSSION

A. Rotational relaxation rates

In a previous study, three PDI probes, including dpPDI and tbPDI, were used to assess spatially heterogeneous dynamics in glycerol. The extracted hydrodynamic volumes were found to run counter to what was initially expected: although tbPDI has the largest molecular weight and space filling volume of the three probes used, it demonstrated the fastest rotational relaxation and in turn had the smallest extracted V_h. Indeed, dpPDI's V_h was found to be more than 5 times larger than that of tbPDI even though tbPDI has a van der Waals volume that is nearly 25% larger than does dpPDI (Table III). We speculated that steric hindrance from the *tert*-butyl groups on tbPDI precludes the hydrogen-bonding interactions that could occur between glycerol and other PDI probes. We predicted that in OTP these two probes would show the opposite behavior, with tbPDI being slower than dpPDI and therefore yielding a larger extracted V_h. As shown in Fig. 2 and Table III, this is indeed the finding in OTP, where the extracted hydrodynamic volumes for tbPDI, dpPDI, and egPDI are 1.87, 1.17, and 0.80 nm^3, respectively. These extracted hydrodynamic volumes reflect the fact that $\tau_{c,med,tbPDI} > \tau_{c,med,dpPDI} > \tau_{c,med,egPDI}$ at all measured temperatures.

While the findings for the relative rotational relaxation rates and hydrodynamic volumes of tbPDI and dpPDI in OTP are in accord with these probes' molecular weights, we note that egPDI has the shortest rotational relaxation time and smallest extracted hydrodynamic volume of the three probes even though its molecular weight is greater than that of dpPDI. To explain this finding, we consider additional measures of probe size and shape. The van der Waals volumes (V_v) of tbPDI, dpPDI, and egPDI are 0.67, 0.46, and 0.54 nm^3, respectively, as computed with ChemBio3D via a Connolly excluded volume calculation. The extracted hydrodynamic volumes of the three probes are larger than the calculated van der Waals volumes in all cases (Table III). The ratio of V_h to V_v for egPDI is the closest to unity, with $V_{h(egPDI,OTP)}$:$V_{v(egPDI)} = 1.48$ while $V_{h(tbPDI,OTP)}$:$V_{v(tbPDI)} = 2.77$ and $V_{h(dpPDI,OTP)}$:$V_{v(dpPDI)} = 2.54$. The fact that egPDI rotates more quickly than the smaller, less massive dpPDI suggests that its rotations may be governed by its core, with the extended hydrocarbon chains providing little hindrance to molecular rotation whereas the bulky phenyl groups of tbPDI and dpPDI may cause more hydrodynamic drag in OTP, slowing their rotational dynamics. The van der Waals volume of the core of the PDI probes is 0.26 nm^3, which would yield $V_{h(egPDI,OTP)}$:$V_{v(egPDI,core)} = 3.08$, quite similar to that for the other two probes. Additional differences between V_h and V_v for all probes likely emerge because of the assumption of a spherical probe in the DSE equation.

V_h may additionally differ from V_v due to the degree of intermolecular forces between the probe and host. Although $V_{h(dpPDI,OTP)}$:$V_{v(dpPDI)}$ is not unity, it is much smaller than that ratio for dpPDI in glycerol, $V_{h(dpPDI,glycerol)}$:$V_{v(dpPDI)} = 4.39$

(Table III). This is consistent with the idea proposed (but not endorsed) by Zondervan *et al.* that strong intermolecular interactions such as hydrogen bonding between PDIs and glycerol can lead to a temporary glycerol shell around the probe, resulting in an effective probe with a larger size and slower rotations than the bare probe.[12] dpPDI's presumed hydrogen-bonding interactions with glycerol slow its rotations in glycerol by a much greater degree than dpPDI's interactions with OTP. If tbPDI cannot hydrogen-bond with glycerol, as proposed, it would lack the glycerol shell and have a smaller V_h:V_v in glycerol, as was found (Table III).[12,14] We note that the discrepancy between the V_h:V_v ratios for tbPDI in glycerol and OTP is not fully understood, as tbPDI in glycerol appears to relax more quickly than would be expected in glycerol even for the bare probe.

B. Reports of heterogeneous dynamics

1. Breadth of relaxation times

One of the key observations emerging from the previous SM study in glycerol was that as probe median rotational correlation time in glycerol decreased, the breadth of reported rotational relaxation times increased.[14] This suggested that as the rate of rotational relaxation of the probe approaches that of the host, the probe can sample and report a greater proportion of the true heterogeneous dynamics of the host. In other words, faster probes do less temporal averaging over these dynamically heterogeneous systems, which leads to an increase in the breadth of distribution of τ_c values. In the study in glycerol, as described above, the fastest probe happened to be that with the highest molecular weight and space filling volume. This implied that within the set of probes used, the differences in rotational relaxation rate, not space filling volume, were most important in setting the breadth of heterogeneous dynamics reported. These results further suggest that at least a subset of dynamic exchanges occur on time scales similar to that of probe rotation.

The same trend found in glycerol is found in OTP, with FWHM of τ_c distributions increasing monotonically with decreasing probe $\tau_{c,med}$ even when this relaxation time does not track with probe molecular weight or van der Waals volume. Of the three dyes studied in OTP, egPDI, the fastest rotating probe, has the largest FWHM of τ_c values across all temperatures studied (Table I and Fig. 3). To highlight this point, Fig. 5(a) shows the histograms also shown in the right panel of Fig. 3 overlaid for all three probes in OTP together with best-fit Gaussians to the $\log(\tau_c)$ histograms. In this case, the Gaussian fits are performed with fixed amplitude and zero offset. FWHM increases as τ_c decreases, with egPDI demonstrating the widest distribution of τ_c values as well as the shortest average rotational correlation time. The fastest rotating probe is also that which exhibits dynamics on a time scale most similar to the structural relaxation of the host: for the three PDI probes in OTP, this ratio ranges from $\tau_c/\tau_\alpha = 168$ for egPDI to $\tau_c/\tau_\alpha = 297$ for tbPDI (Table III). Determination of τ_c/τ_α values is described in the supplementary material.[28] As in glycerol, the fact that the faster probe reports the greatest breadth of heterogeneity supports the idea that at least a proportion of the dynamic exchange occurs on time scales similar to those associated with probe rotation.

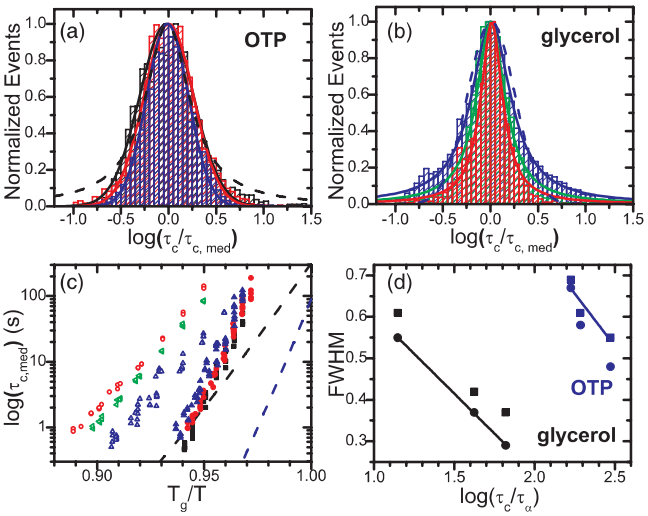

FIG. 5. SM data from all temperatures normalized and combined to form a single histogram for (a) each PDI in OTP: tbPDI (blue), dpPDI (red), and egPDI (black) and (b) each PDI in glycerol: dpPDI (red), dapPDI (green), and tbPDI (blue). All histograms are normalized to their maximum number of occurrences. Each PDI in OTP histogram is fit with a fixed height Gaussian and each PDI in glycerol histogram is fit with a fixed-height Lorentzian (lines of solid colors corresponding to histogram colors). The histogram for egPDI in OTP is additionally fit with a fixed-height Lorentzian (black dashed line in a) and tbPDI in glycerol is fit with a fixed-height Gaussian (blue dashed line in b). (c) $\tau_{c,med}$ from each movie plot with respect to T_g/T for egPDI (black squares), dpPDI (red circles), and tbPDI (blue triangles) in OTP and tbPDI (open blue triangles), dapPDI (open green sideways triangle), and dpPDI (open red circles) in glycerol. Structural relaxation data for OTP (dashed blue line)[30] and glycerol (dashed black line)[29] are plot with respect to T_g/T. (d) FWHM from Gaussian (squares) and Lorentzian (circles) fits to each of the OTP (blue) and glycerol (black) histograms pictured in (a) and (b) plot as a function $\log(\tau_c/\tau_\alpha)$. FWHM from Gaussian fits of OTP (blue squares) and from Lorentzian fits of glycerol (black circles) τ_c distributions vs. $\log(\tau_c/\tau_\alpha)$ are fit to lines. y-intercepts correspond to FWHM for $\tau_c/\tau_\alpha = 1$.

We may also consider the breadth of heterogeneity reported by these probes in OTP compared to in glycerol. Taking the same data shown in Fig. 2 as well as that for 3 PDI probes in glycerol and plotting it as a function of T/T_g – as in an Angell plot – reinforces that in both cases probes follow the dynamics of the host, here as captured by structural relaxation data measured for OTP and glycerol[29,30] (Fig. 5(c)). From this plot, it is also apparent that OTP dynamics (and probe reports of said dynamics) change more quickly with temperature than do those of glycerol over the same temperature range relative to T_g. This highlights the fact that OTP is more fragile than glycerol, with fragility a measure of the degree of non-Arrhenius change in viscosity with temperature upon approach to T_g.[1,24] It has been proposed that more fragile systems may display a greater degree of heterogeneous dynamics than less fragile ones,[4,24] and we investigate whether our results provide evidence for different degrees of heterogeneous dynamics in OTP and glycerol.

Figures 5(a) and 5(b) show the combined histograms across temperatures for three probes in OTP and glycerol, respectively. In both cases, best-fit amplitude-fixed and zero-offset Gaussian and Lorentzian fits are performed. While all

fits are relatively good, the Gaussian fits better describe the summed OTP histograms ($R^2 = 0.98$ for all probes for Gaussian fits vs. 0.92-0.95 for Lorentzian fits) while the Lorentzian fits better describe the summed glycerol τ_c histograms ($R^2 = 0.91$-0.99 for all probes for Gaussian fits vs. 0.97-0.99 for Lorentzian fits). Considering either Gaussian or Lorentzian fits, the τ_c histograms measured in OTP are broader than those measured in glycerol (Fig. 5(d)). While probes in OTP tend to display shorter trajectories in terms of probe τ_c than in glycerol, egPDI in OTP and dapPDI in glycerol have nearly identical average trajectory lengths of 98 and $102\tau_c$, respectively. Thus, simulation of homogeneous rotational diffusion in both cases yields FWHM values of $\log(\tau_c)$ distributions of 0.34. The experimental FWHM values, on the other hand, are 0.69 for egPDI in OTP and 0.42 for dapPDI in glycerol, with the corresponding τ_c/τ_α values being 168 and 42, respectively (Table III). The fact that a broader τ_c distribution is found in OTP even though this probe is performing a greater degree of temporal averaging than the corresponding probe in glycerol suggests that OTP is more heterogeneous than glycerol. We note that it was initially expected that τ_c/τ_α values for PDIs in OTP would be closer to unity and indeed smaller than those in glycerol. This assumption was based on the fact that OTP molecules are larger than glycerol molecules, and PDI probes are closer in molecular weight and van der Waals volume to OTP than to glycerol molecules. That this is clearly not the case is suggestive of the fact that glycerol, with its hydrogen bonding network, may have a larger effective relaxing unit (perhaps related to cooperatively rearranging sets of molecules) than does OTP.

Figure 5(d) displays the FWHM values of the τ_c distributions of all probes in both glycerol and OTP as a function of $\log(\tau_c/\tau_\alpha)$. In both supercooled liquids the FWHM values of the probe distributions increase with decreasing $\log(\tau_c/\tau_\alpha)$. Extrapolating linear fits of this data to $\tau_c/\tau_\alpha = 1$ (i.e., where probe rotational correlation time is equal to the host structural relaxation time) implies a situation in which no temporal averaging by the probe would be expected. For glycerol, in this limit, the extrapolated FWHM is 0.99 while that of OTP is 1.80. We suggest this is additional evidence that OTP exhibits a greater degree of spatially heterogeneous dynamics than glycerol. We note, however, that other possibilities also exist. First, it has been suggested that OTP has larger regions of distinct dynamics than glycerol.[31–33] The employed probes, with radii along the transition dipole of ≈0.2 nm, are more likely to span regions of distinct dynamics in glycerol than in OTP. This could lead to more spatial averaging by the employed PDI probes in glycerol than in OTP, which could contribute to differences in the widths of the histograms in the two supercooled liquids. Another possibility is that dynamic exchange occurs on quite different time scales in OTP and glycerol. Indeed, while several experiments suggest that dynamic exchange happens on time scales similar to structural relaxation in glycerol and OTP,[21–23,34] at least one experiment suggests very long-lived heterogeneity in glycerol.[12] If glycerol and OTP have dissimilar characteristic time scales of dynamic exchange (τ_{ex}) relative to the structural relaxation time, the τ_c/τ_{ex} ratio would be decoupled from the τ_c/τ_α ratio and extrapolation to $\tau_c/\tau_\alpha = 1$ may not equally correct for temporal averaging in OTP and glycerol.

2. Evaluation of stretching exponent

Just as distributions of probe τ_c values reveal information about host heterogeneous dynamics, so too may distributions of stretching exponents. As described in Sec. III B 2, the β_{med} values in OTP are close to 1.0, as are those attained from simulations of purely homogeneous dynamics (Figs. 4(a)–4(c) and Table II), likely due in part to the time-limited nature of the SM trajectories. Quasi-ensemble interpretation of stretching exponents, however, shows not only that measured $\beta_{med} > \beta_{QE}$ in OTP for all probes but also that β_{QE} obtained from experiments does differ substantially from that attained from these simulations (Fig. 4(d) and Table II). The finding of $\beta_{med} > \beta_{QE}$ is consistent with the fact that greater differences are observed across probes than within probes over time, or that spatial heterogeneity dominates over temporal heterogeneity in these SM measurements. This is because in the limit of long trajectories, the deviation of β_{med} from 1.0 reports on temporal heterogeneity experienced and reported by a probe while β_{QE} reveals both that temporal heterogeneity plus any differences across probes, i.e., spatial heterogeneity. This conclusion is similar to recent conclusions of Gruebele and co-workers for SM probe-free experiments on a metal glass surface.[35] SM probe report of a greater degree of spatial than temporal heterogeneity is consistent with the spread of τ_c values being larger than expected from simulation of homogeneous dynamics while the distribution of individual β values does not differ substantially from that obtained from those simulations. We note that SM probe reports of a greater degree of spatial than temporal heterogeneity does not necessarily imply this is true of the supercooled OTP itself; indeed, the fact that data collected in both OTP and glycerol show that the fastest probes report the greatest breadth of heterogeneity strongly suggests dynamic exchange on (and likely below) the time scale of probe rotations occurs in these supercooled liquids. The probe-dependent findings further suggest that extrapolating to the limit of no temporal averaging (Fig. 5(d)) can yield important information of instantaneous (spatial) heterogeneity in a supercooled liquid.

As described in Sec. III B 2, to compare β values obtained from SM experiments to those obtained from ensemble studies, a β_{QE} value is extracted from ACF_{QE}s for each type of PDI probe measured in OTP. β_{QE} values remain relatively constant across temperature for all probes studied in OTP, as for FWHM values of τ_c distributions. The fastest rotating probe in OTP, egPDI, exhibits the smallest β_{QE} value with an average $\beta_{QE} = 0.78$ across temperatures. This value is larger than that obtained from probe-free measurements in OTP where $\beta \approx 0.35$–0.50.[30,36] However, it is similar to those obtained from most probe-bearing experiments in OTP, which yield β values from 0.60–0.90, some of which show temperature dependence in the temperature regime investigated here.[31,37,38] In these measurements, potential probe averaging in space and time cannot be distinguished. In our

measurements, in which the fastest probes consistently report the greatest degree of host heterogeneity regardless of probe size, the increase in β_{QE} values relative to β values measured in probe-free experiments points to the importance of temporal averaging rather than spatial averaging by these probes, as has been suggested previously.[39–41]

In analogy with the FWHM values obtained from τ_c distributions extrapolated to $\tau_c/\tau_\alpha = 1$, the value of β_{QE} in the limit of no temporal averaging can be estimated. Doing so reinforces that time-limited trajectories affect extracted β values more substantially than FWHM values of τ_c distributions, as described previously.[17] For all probes in OTP, β_{med} is near 1.0 and $\beta_{med} > \beta_{QE}$. This is true, as well, for measurements of dpPDI, dapPDI, and tbPDI in glycerol. In Figure 6, β_{QE} values are plot as a function of probe and trajectory length for every movie collected in OTP and glycerol. For the employed probes, probe lifetime in glycerol is significantly longer than in OTP. For dpPDI and dapPDI in glycerol, β_{QE} values exhibit a plateau at a value of $\beta_{QE} \approx 0.9$, regardless of trajectory length. On the other hand, the tbPDI β_{QE} decreases with increasing trajectory length. In OTP, it is not clear whether any of the probes exhibit a plateau, and it appears that the two faster rotating probes, dpPDI and egPDI, show a trend towards lower β_{QE} with increasing trajectory length. For simulations of homogenous rotational dynamics and those with spatial but no temporal heterogeneity, it was previously shown that decreases in β_{QE} occur as a function of trajectory length for trajectories of up to $1000\tau_c$; however, most of the change occurs below $100\tau_c$ even though the FWHM of τ_c distributions evolves little in this same trajectory length range.[17] For a system with temporal heterogeneity, additional decrease of β_{QE} with increasing trajectory length may be expected as each individual SM ACF becomes increasingly stretched for probes that do not substantially average over dynamic heterogeneities in these systems. We find evidence for this occurring for tbPDI in glycerol and egPDI in OTP. Because of the short trajectories of the other two probes in OTP, the β_{QE} values may not accurately represent the degree of heterogeneity in the supercooled liquid. This is illustrated by Fig. 6(b), where average β_{QE} values averaged over all movies for each probe are plot vs. FWHM of τ_c distributions. In both cases, the relationship between FWHM and β_{QE} is approximately linear. For glycerol, extrapolating to FWHM = 0.99, the value at which probe rotational correlation time is equivalent to host structural relaxation time, β_{QE} is 0.48, very similar to that obtained from ensemble experiments.[42] The same approach for OTP, however, yields an unphysical, negative β_{QE} value, likely because the β_{QE} values are overestimated, particularly for dpPDI and tbPDI due to the short trajectories collected. Despite this, the approximately linear relationship between FWHM and β_{QE} for both glycerol and OTP provides evidence that both quantities are reporting on the same spatially heterogeneous dynamics in the host supercooled liquids.

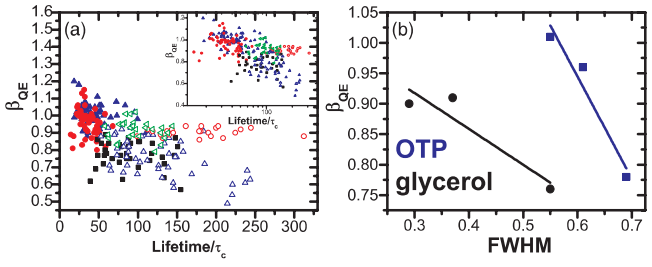

FIG. 6. (a) β_{QE} with respect to median trajectory length in terms of $\tau_{c,med}$ for each measurement for egPDI (black squares), dpPDI (red circles), and tbPDI (blue triangles) in OTP and tbPDI (open blue triangles), dapPDI (open green sideways triangles), and dpPDI (open red circles) in glycerol. Inset shows the same data with trajectory length plot on a log scale. (b) Average β_{QE} for each PDI studied in OTP (blue) or glycerol (black) with respect to FWHM from Gaussian (OTP) or Lorentzian (glycerol) fits to each histogram pictured in Figs. 5(a) and 5(b) as well as best-fit lines to the data.

V. CONCLUSIONS

This study monitored the rotational relaxation dynamics of three PDI probes in OTP near the glass transition temperature. Each of the three probes sampled and reported rotational correlation times that spanned more than a decade, consistent with the presence of spatially heterogeneous dynamics in OTP. As in glycerol, probe rotational correlation time scaled inversely with breadth of SM τ_c distribution, with faster probes having a broader τ_c distribution. This implies that a portion of the full range of dynamic exchange events occurs on probe rotational correlation time scales. For these probes in OTP, the τ_c/τ_α value is on the order of 100 and thus dynamic exchange reported by these probes is occurring on similar time scales. Extrapolating FWHM of rotational relaxation times to the α-relaxation time of the host suggests that the τ_c distribution would span approximately two decades if an instantaneous measurement could be performed. Comparison with SM measurements in glycerol suggests that the more fragile OTP is more spatially heterogeneous than is glycerol, though discrepancies between reports of heterogeneity from τ_c distributions and those from evaluating stretching exponents require additional study. This SM study in OTP not only confirms findings from previous study in glycerol suggesting dynamic exchange occurs on and below the probe rotational time scales, it also demonstrates how probe-dependent studies can be used to extrapolate to a regime in which effects of temporal averaging are eliminated, an important consideration when employing probes to interrogate dynamically heterogeneous systems.

ACKNOWLEDGMENTS

This research was supported by the National Science Foundation (NSF) under Grant Nos. CHE 0744322, DGE 0801530, and an NSF GRF for L.M.L. We thank L. Campos and co-workers for supplying egPDI. We thank S. Snyder for assistance with ChemBio3D. We thank Keewook Paeng for valuable discussions.

[1]C. A. Angell, "Formation of glasses from liquids and biopolymers," Science **267**, 1924–1935 (1995).
[2]M. D. Ediger, C. A. Angell, and S. R. Nagel, "Supercooled liquids and glasses," J. Phys. Chem. **100**, 13200–13212 (1996).
[3]P. G. Debenedetti and F. H. Stillinger, "Supercooled liquids and the glass transition," Nature (London) **410**, 259–267 (2001).
[4]M. D. Ediger, "Spatially heterogeneous dynamics in supercooled liquids," Annu. Rev. Phys. Chem. **51**, 99–128 (2000).

[5]R. Richert, "Heterogeneous dynamics in liquids: Fluctuations in space and time," J. Phys.: Condens Matter **14**, R703–R738 (2002).
[6]G. Adam and J. H. Gibbs, "On temperature dependence of cooperative relaxation properties in glass-forming liquids," J. Chem. Phys. **43**, 139–147 (1965).
[7]L. Berthier, G. Biroli, J. P. Bouchaud, L. Cipelletti, D. El Masri, D. L'Hote, F. Ladieu, and M. Pierno, "Direct experimental evidence of a growing length scale accompanying the glass transition," Science **310**, 1797–1800 (2005).
[8]L. Berthier and G. Biroli, "Theoretical perspective on the glass transition and amorphous materials," Rev. Mod. Phys. **83**, 587–645 (2011).
[9]H. Sillescu, R. Bohmer, G. Diezemann, and G. Hinze, "Heterogeneity at the glass transition: What do we know?," J. Non-Cryst. Sol. **307–310**, 16–23 (2002).
[10]R. Bohmer, R. V. Chamberlin, G. Diezemann, B. Geil, A. Heuer, G. Hinze, S. C. Kuebler, R. Richert, B. Schiener, H. Sillescu, H. W. Spiess, U. Tracht, and M. Wilhelm, "Nature of the non-exponential primary relaxation in structural glass-formers probed by dynamically selective experiments," J. Non-Cryst. Sol. **235–237**, 1–9 (1998).
[11]L. A. Deschenes and D. A. V. Bout, "Heterogeneous dynamics and domains in supercooled o-terphenyl: A single molecules study," J. Phys. Chem. B **106**, 11438–11445 (2002).
[12]R. Zondervan, F. Kulzer, G. C. G. Berkhout, and M. Orrit, "Local viscosity of supercooled glycerol near T_g probed by rotational diffusion of ensembles and single dye molecules," Proc. Natl. Acad. Sci. U.S.A. **104**, 12628–12633 (2007).
[13]S. A. Mackowiak, T. K. Herman, and L. J. Kaufman, "Spatial and temporal heterogeneity in supercooled glycerol: Evidence from wide field single molecule imaging," J. Chem. Phys. **131**, 244513 (2009).
[14]S. A. Mackowiak, L. M. Leone, and L. J. Kaufman, "Probe dependence of spatially heterogeneous dynamics in supercooled glycerol as revealed by single molecule microscopy," Phys. Chem. Chem. Phys. **13**, 1786–1799 (2011).
[15]L. J. Kaufman, "Heterogeneity in single-molecule observables in the study of supercooled liquids," Annu. Rev. Phys. Chem. **64**, 177–200 (2013).
[16]C. Y. Lu and D. A. Vanden Bout, "Effect of finite trajectory length on the correlation function analysis of single molecule data," J. Chem. Phys. **125**, 124701 (2006).
[17]S. A. Mackowiak and L. J. Kaufman, "When the heterogeneous appears homogeneous: Discrepant measures of heterogeneity in single-molecule observables," J. Phys. Chem. Lett. **2**, 438–442 (2011).
[18]A. Schob, F. Cichos, J. Schuster, and C. von Borczyskowski, "Reorientation and translation of individual dye molecules in a polymer matrix," Eur. Polym. J. **40**, 1019–1026 (2004).
[19]D. Bingemann, R. M. Allen, and S. W. Olesen, "Single molecules reveal the dynamics of heterogeneities in a polymer at the glass transition," J. Chem. Phys. **134**, 024513 (2011).
[20]S. Adhikari, M. Selmke, and F. Cichos, "Temperature dependent single molecule rotational dynamics in PMA," Phys. Chem. Chem. Phys. **13**, 1849–1856 (2011).
[21]M. T. Cicerone and M. D. Ediger, "Relaxation of spatially heterogeneous dynamic domains in supercooled ortho-terphenyl," J. Chem. Phys. **103**, 5684–5692 (1995).
[22]R. Bohmer, G. Hinze, G. Diezemann, B. Geil, and H. Sillescu, "Dynamic heterogeneity in supercooled ortho-terphenyl studied by multidimensional deuteron NMR," Europhys. Lett. **36**, 55–60 (1996).
[23]C. Y. Wang and M. D. Ediger, "How long do regions of different dynamics persist in supercooled o-terphenyl?," J. Phys. Chem. B **103**, 4177–4184 (1999).
[24]C. A. Angell, "Relaxation in liquids, polymers and plastic crystals - strong fragile patterns and problems," J. Non-Cryst. Sol. **131–133**, 13–31 (1991).
[25]T. K. Herman, S. A. Mackowiak, and L. J. Kaufman, "High power light emitting diode based setup for photobleaching fluorescent impurities," Rev. Sci. Instrum. **80**, 016107 (2009).
[26]D. Bingemann, "Analysis of 'blinking' or 'hopping' single molecule signals with a limited number of transitions," Chem. Phys. Lett. **433**, 234–238 (2006).
[27]W. T. Laughlin and D. R. Uhlmann, "Viscous flow in simple organic liquids," J. Phys. Chem. **76**, 2317–2325 (1972).
[28]See supplementary material at http://dx.doi.org/10.1063/1.4773889 for details of the heating correction procedure.
[29]N. B. Olsen, T. Christensen, and J. C. Dyre, "Time-temperature superposition in viscous liquids," Phys. Rev. Lett. **86**, 1271–1274 (2001).
[30]R. Richert, "On the dielectric susceptibility spectra of supercooled o-terphenyl," J. Chem. Phys. **123**, 154502 (2005).
[31]M. T. Cicerone, F. R. Blackburn, and M. D. Ediger, "How do molecules move near T_g - molecular rotation of 6 probes in o-terphenyl across 14 decades in time," J. Chem. Phys. **102**, 471–479 (1995).
[32]S. A. Reinsberg, X. H. Qiu, M. Wilhelm, H. W. Spiess, and M. D. Ediger, "Length scale of dynamic heterogeneity in supercooled glycerol near T_g," J. Chem. Phys. **114**, 7299–7302 (2001).
[33]S. A. Reinsberg, A. Heuer, B. Doliwa, H. Zimmermann, and H. W. Spiess, "Comparative study of the NMR length scale of dynamic heterogeneities of three different glass formers," J. Non-Cryst. Sol. **307–310**, 208–214 (2002).
[34]B. Schiener, R. V. Chamberlin, G. Diezemann, and R. Bohmer, "Nonresonant dielectric hole burning spectroscopy of supercooled liquids," J. Chem. Phys. **107**, 7746–7761 (1997).
[35]S. Ashtekar, J. Lyding, and M. Gruebele, "Temperature-dependent two-state dynamics of individual cooperatively rearranging regions on a glass surface," Phys. Rev. Lett. **109**, 166103 (2012).
[36]F. Fujara, B. Geil, H. Sillescu, and G. Fleischer, "Translational and rotational diffusion in supercooled orthoterphenyl close to the glass-transition," Z. Phys. B: Condens. Matter **88**, 195–204 (1992).
[37]M. K. Mapes, S. F. Swallen, and M. D. Ediger, "Self-diffusion of supercooled o-terphenyl near the glass transition temperature," J. Phys. Chem. B **110**, 507–511 (2006).
[38]S. Y. Grebenkin and B. V. Bol'shakov, "Rotational mobility of guest molecules in o-terphenyl below T_g," J. Phys. Chem. B **110**, 8582–8586 (2006).
[39]M. Yang and R. Richert, "Solvation dynamics and probe rotation in glass-forming liquids," Chem. Phys. **284**, 103–114 (2002).
[40]L. M. Wang and R. Richert, "Exponential probe rotation in glass-forming liquids," J. Chem. Phys. **120**, 11082–11089 (2004).
[41]W. Huang and R. Richert, "Dielectric study of probe rotation in viscous liquids," Philos. Mag. **87**, 371–382 (2007).
[42]K. Schroter and E. Donth, "Viscosity and shear response at the dynamic glass transition of glycerol," J. Chem. Phys. **113**, 9101–9108 (2000).